Ultrastrong waveguide QED with giant atoms

Sergi Terradas-Briansó,[1] Carlos A. González-Gutiérrez,[1] Franco Nori,[2,3,4] Luis Martín-Moreno,[1] and David Zueco[1]
[1]*Instituto de Nanociencia y Materiales de Aragón, CSIC, Universidad de Zaragoza, Zaragoza 50009, Spain*
[2]*Department of Physics, University of Michigan, Ann Arbor, Michigan 48109-1040, USA*
[3]*Theoretical Quantum Physics Laboratory, RIKEN Cluster for Pioneering Research, Wako-shi, Saitama 351-0198, Japan*
[4]*RIKEN Center for Quantum Computing, 2-1 Hirosawa, Wako-shi, Saitama 351-0198, Japan*

(Received 16 June 2022; accepted 4 November 2022; published 22 December 2022)

Quantum optics with giant emitters has shown a new route for the observation and manipulation of non-Markovian properties in waveguide QED. In this paper we extend the theory of giant atoms, hitherto restricted to the perturbative light-matter regime, to deal with the ultrastrong-coupling regime. Using static and dynamical polaron methods, we address the low-energy subspace of a giant atom coupled to an Ohmic waveguide beyond the standard rotating-wave approximation. We analyze the equilibrium properties of the system by computing the atomic frequency renormalization as a function of the coupling characterizing the localization-delocalization quantum phase transition for a giant atom. We show that virtual photons dressing the ground state are nonexponentially localized around the contact points but decay as a power law. The dynamics of an initially excited giant atom is studied, pointing out the effects of ultrastrong coupling on the Lamb shift and the spontaneous emission decay rate. Finally, we comment on the existence of the so-called oscillating bound states beyond the rotating-wave approximation.

DOI: 10.1103/PhysRevA.106.063717

I. INTRODUCTION

The coupling of a single quantum emitter to a continuum of electromagnetic modes has been an important problem since the birth of quantum theory [1]. Current experiments, involving different technological platforms, have shown that propagating photons can be coupled efficiently to localized quantum emitters. This field, known as waveguide quantum electrodynamics, has received a great deal of attention due to the interesting theoretical and experimental applications [2–4]. In most scenarios, emitters are described as pointlike particles of negligible size compared to the wavelength of the electromagnetic radiation. This justifies the standard dipole approximation widely employed in quantum optics. In recent years, however, experiments involving artificial emitters coupled at different points to a waveguide have required going beyond the treatment of emitters as pointlike matter coupling locally to a waveguide. This comes as a consequence of the distance between coupling points, which can reach lengths of the order of or larger than the characteristic wavelength of the electromagnetic radiation [5,6]. In the literature, these type of emitters are called giant atoms. As a consequence of the nonlocal light-matter interaction, remarkable phenomena have been reported. Examples are non-Markovian dynamics [6–10], tunable decay rates and Lamb shifts [11–13], tunable couplings [14], structure-waveguide-mediated atom-atom interactions [15], engineering of energy levels [16], and bound states emerging from interference between coupling points, including oscillating [17,18] and chiral [19] bound states. In addition, bound states originating from photonic band edges for giant atoms have been studied in [20]. The large size of the system also allows for a giant emitter to be coupled to a waveguide in between the connection points of other giant atoms. The many possible configurations can lead to decoherence-free interactions between giant emitters [12,13] or nonreciprocal excitation transfer [21]. See Ref. [22] for a recent overview of the field.

The breakdown of the dipolar approximation leads to the appearance of deviations from Markovian dynamics. These typically arise from the coupling of quantum emitters to structured environments with nonflat spectral functions [23–25]. However, it has been shown that retardation effects can induce strong non-Markovian features whenever coherent feedback is allowed to influence the dynamics [26–33]. Giant emitters fall naturally into this last category of non-Markovian systems [22] and they have been a relevant topic in waveguide QED systems.

Another assumption that is being reconsidered, due to experiments, is the fact that photons are weakly coupled to matter, so their interaction can be described in a perturbative way. Several experiments have reached the so-called ultrastrong-coupling (USC) regime between light and single quantum emitters, in both cavity [34–36] and waveguide QED [37–39]. In the USC regime higher-order processes, rather than the creation (annihilation) of one photon by annihilating (creating) one matter excitation, play a role. Then the rotating-wave approximation (RWA) for the interaction breaks down, the atomic bare parameters get renormalized, and the ground state becomes nontrivial. This has interesting consequences. Some of them are the possibility of transforming virtual photons onto real photons by perturbing the ground state [40–45], the localization-delocalization transition [46,47], or

2469-9926/2022/106(6)/063717(13)

the possibility to perform nonlinear optics at the single- and zero-photon limit [48–53]. Reviews for light-matter interactions in the USC regime can be found in [54,55].

In this work we discuss the low-energy physics (both at and out of equilibrium) of a giant atom coupled to a continuum in the USC regime. To do so, the light-matter coupling is treated within the spin-boson model. In the USC this is a paradigmatic example of a nonanalytically solvable model [56]. Different techniques are available in the literature to deal with it, such as matrix-product states [46,48,49], density-matrix renormalization-group methods [57], hierarchical equations of motion or pseudomodes methods [58], and path integral [59–61], polaronlike [47,62–67], or Gaussian approaches [68]. It was recently reported [69] how to use matrix-product states to describe the dynamics of giant atoms in a waveguide in the USC regime.

In this paper we employ polaronlike techniques, complementing and extending their work. We examine the renormalization of atomic parameters and provide expressions for them. We prove the existence of the localization-delocalization transition in giant emitters, as well as a profile of the virtual photons in the ground state which we characterize for both phases. Regarding the dynamics, we discuss the spontaneous emission, its rate, and the Lamb shift in the USC regime. Within the non-Markovian regime we provide numerical results and analytical expressions for the emission and the existence of bound states, also oscillating ones.

The rest of the paper is organized as follows. In Sec. II we introduce the theoretical model, including the discrete model for the waveguide as well as the spin-boson Hamiltonian and spectral density of the system. In Sec. III we describe the polaron formalism and apply it to our model to reach the effective Hamiltonian used throughout the work. In Sec. IV we analyze the equilibrium properties of the system, including its ground state and renormalization of the transition energy leading to the discussion of the quantum phase transition. In Sec. V we compute the Lamb-Shift and effective decay rate for the system. In Sec. VI we study different cases of the non-Markovian dynamics of the system, using numerical simulations and approximate analytical expressions with particular focus on oscillating bound states. Finally, a summary and conclusions of this work are given in Sec. VII.

II. SPIN-BOSON MODEL FOR A GIANT EMITTER

We start by introducing the Hamiltonian of the system, described schematically in Fig. 1(a),

$$H = H_q + H_{\rm wg} + H_{\rm int}. \tag{1}$$

Here $H_q = (\Delta/2)\sigma^z$ is the Hamiltonian of the two-level system with transition frequency Δ between its ground state $|g\rangle$ and excited state $|e\rangle$; $H_{\rm wg}$ is the Hamiltonian modeling the waveguide and $H_{\rm int}$ accounts for the qubit-waveguide interaction. The waveguide is modeled by using the discrete transmission line shown in Fig. 1(b). This covers several current realizations with superconducting qubits, as reported in Refs. [12,13]. The waveguide modes are found by diagonalizing the corresponding microscopic circuit model via the standard procedure based on [70] (see Appendix A for a detailed derivation). The Hamiltonian of the waveguide is

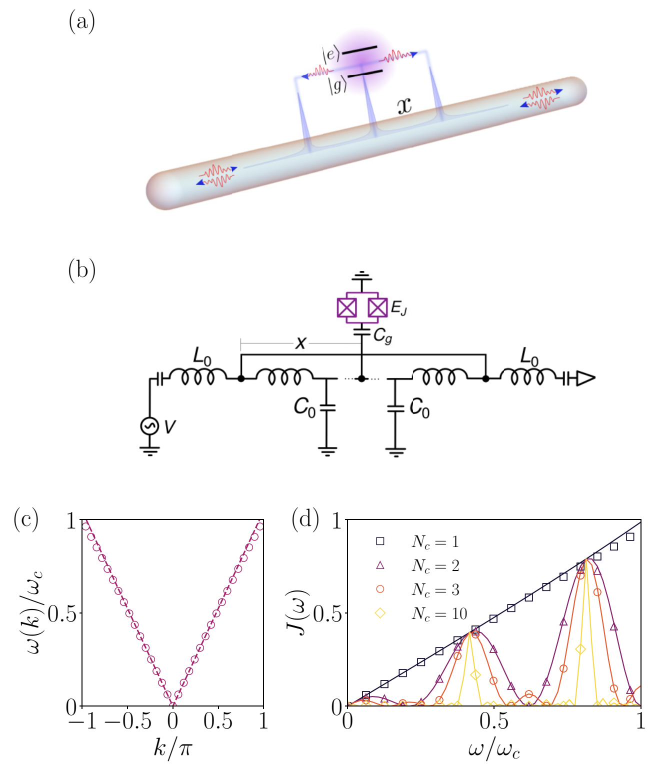

FIG. 1. (a) Pictorial illustration of the giant emitter with three connection points. (b) Schematic of a circuit-QED implementation of a giant atom coupled to an Ohmic waveguide with three connection points. (c) Dispersion relations for the discrete and continuous models for the Ohmic waveguide. The group velocity for the waveguide is $v_g = c = 1$ throughout this work. (d) Spectral function $J(\omega)$ for a continuous dispersion relation $\omega_k = v_g|k|$ shown by solid lines and the corresponding results using the dispersion relation from Eq. (3) for $N_c = 1$ (squares), $N_c = 2$ (triangles), $N_c = 3$ (circles), and $N_c = 10$ (diamonds). The spacing between coupling points is $x = 5\delta x$ and the coupling strength $\alpha = 0.1$. The cutoff frequency is $\omega_c = 3$ and the number of modes is $N = 300$ for both plots (c) and (d).

then given by

$$H_{\rm wg} = \sum_k \omega_k a_k^\dagger a_k. \tag{2}$$

In this procedure we choose a discretization length $\delta x = L/N$, with L the length of the transmission line and N the number of propagating modes. For a linear medium in one dimension, discretization yields the LC chain, with the set of momenta $k_n = 2\pi n/L,\ n \in \{-N/2, \dots, N/2\}$, and the dispersion relation

$$\omega_k = \omega_c\sqrt{2 - 2\cos(k_n\delta x)}, \tag{3}$$

where $\omega_c = v_g/\delta x$ is the cutoff frequency, with v_g the group velocity of the propagating photons. The extended nature of the giant atom is incorporated in the interaction Hamiltonian. We assume that this interaction is established via the simultaneous coupling of the two-level system to a set of contact points in the waveguide [see Fig. 1(b)]. The interaction

Hamiltonian reads

$$H_{\text{int}} = \sigma^x \sum_{j=1}^{N_c} \sum_k \frac{g_k}{N_c} (a_k e^{ikx_j} + \text{H.c.}). \tag{4}$$

Here $g_k = g\sqrt{\omega_k/2L}$ are frequency-dependent couplings, with $g = \sqrt{\pi v_g \alpha}$, and α is the dimensionless coupling parameter. In addition, N_c is the total number of contact points at positions x_j and $1/N_c$ is a normalization factor chosen to ensure that in the zero-distance limit the model reduces to the standard small-atom case with the appropriate coupling strength. This facilitates the comparison for different N_c having a well-defined limit as $N_c \to \infty$. We can now write down the complete Hamiltonian (1) in the form of a spin-boson-like model [71]

$$H = \frac{\Delta}{2}\sigma^z + \sum_k \omega_k a_k^\dagger a_k + \sigma^x \sum_k (\tilde{g}_k a_k + \text{H.c.}), \tag{5}$$

with effective coupling functions

$$\tilde{g}_k = \frac{g_k}{N_c} \sum_{j=1}^{N_c} e^{ikx_j}. \tag{6}$$

The Hamiltonian (5) is a general effective description for a giant atom in interaction with a waveguide. For completeness, readers are referred to Appendix A for its derivation from the specific circuit represented in Fig. 1(b). Spin-boson models are characterized by their spectral function

$$J(\omega) \equiv 2\pi \sum_k |\tilde{g}_k|^2 \delta(\omega - \omega_k). \tag{7}$$

The spectral function encapsulates all the information on the bath frequency modes and their coupling to the two-level system [72]. The discretization we use guarantees that in the continuum limit $N \to \infty$ ($\delta x \to 0$), $\omega_k \approx v_g|k|$ [see Fig. 1(c)] and

$$J(\omega) = J_{\text{Ohm}}(\omega) G(\omega). \tag{8}$$

The Ohmic part $J_{\text{Ohm}}(\omega) = \pi\alpha\omega$ comes from the local coupling to a one-dimensional continuum, while the modulation function

$$G(\omega) = \frac{1}{N_c^2} \sum_{j,l} e^{i\omega(x_j - x_l)/v_g} \tag{9}$$

arises from interference caused by the multiple coupling points. For equidistant contact points with distance x, the modulation function simplifies to

$$G(\omega) = \frac{1}{N_c^2} \frac{1 - \cos(N_c \omega x/v_g)}{1 - \cos(\omega x/v_g)}. \tag{10}$$

Figure 1(d) shows the spectral function of the waveguide and its modification for different N_c, compared to the small emitter limit $N_c = 1$, for both the discrete (open circles) and continuous descriptions of the waveguide (solid lines). The interdistance x is fixed, so the main peaks coincide for all N_c. On the other hand, as the contact points increase, the peaks become narrower with a width proportional to N_c^{-1}.

III. EFFECTIVE RWA MODELS IN THE USC: POLARON THEORY FOR THE GIANT ATOM

The low-energy spectrum of a spin-boson model (5) can be well approximated by an effective excitation-number-conserving Hamiltonian derived from a polaron transformation [64–66]. The polaron transformation seeks to disentangle the atom and waveguide, by choosing a set of variational parameters such that the ground state of the transformed Hamiltonian is as close as possible to $|g\rangle \otimes |\mathbf{0}\rangle$, i.e., to the direct product of the ground state of the uncoupled atom $|g\rangle$ and the ground state of the waveguide $|\mathbf{0}\rangle$. Furthermore, it has been shown to be accurate for various realizations of the spin-boson model, e.g., considering multiple emitters [30,73], and for different functional forms of the spectral function [66]. In this section we summarize the main aspects of the static and dynamical polaron theory in order to proceed with its application to the case at hand, a giant atom beyond the rotating-wave approximation. The polaron transformation is given by

$$U_p = \exp\left(-\sigma^x \sum_k (f_k a_k^\dagger - f_k^* a_k)\right), \tag{11}$$

where f_k is the set of variational parameters.

As mentioned, we choose these variational parameters so that the ground state is approximately $|g\rangle|\mathbf{0}\rangle$. For Eq. (5) this is equivalent to minimize the ground-state energy $\min_{f_k}\{\langle\mathbf{0}|\langle g|\, U_p^\dagger H U_p\, |g\rangle|\mathbf{0}\rangle\}$. For a detailed application of the polaron transformation on the spin-boson Hamiltonian we point the reader to Appendix B. We find that [cf. Eq. (6)]

$$f_k = \frac{\tilde{g}_k}{\omega_k + \Delta_r}, \tag{12}$$

with

$$\Delta_r = \Delta \exp\left(-2 \sum_k |f_k|^2\right). \tag{13}$$

Both Δ_r and f_k are related by a self-consistent equation that can be solved numerically. Once such parameters are found, we can obtain all the properties of the model. Within the scope of the present work, we can restrict our treatment to the low-energy sector, where the polaron model can be well approximated by the effective number-preserving Hamiltonian

$$\begin{aligned} H_p &\approx H_{\text{eff}} \\ &= \frac{\Delta_r}{2}\sigma^z + \sum_k \omega_k a_k^\dagger a_k + 2\Delta_r \sum_k f_k (\sigma^+ a_k + \text{H.c.}) \\ &\quad + V_{\text{local}} + E_{\text{ZP}}, \end{aligned} \tag{14}$$

where $V_{\text{local}} = -2\Delta_r \sigma^z \sum_{k,k'} f_k f_{k'} a_k^\dagger a_{k'}$ and

$$E_{\text{ZP}} = -\frac{\Delta_r}{2} + \sum_k f_k(\omega_k f_k - \tilde{g}_k - \tilde{g}_k^*). \tag{15}$$

In this effective Hamiltonian we can recognize Δ_r in Eq. (13) as a renormalized atomic frequency. This is a well-known consequence in the USC regime [71,73,74]. This renormalization is responsible for the localization-delocalization transition that corresponds to the ferromagnetic-antiferromagnetic phase transition in the Kondo model [75]. In the delocalized phase ($\Delta_r \to 0$), the ground state is degenerated since the atom can be in either the symmetric or antisymmetric superpositions. In the next section we will tackle this renormalization of the atom frequency and the existence of a quantum phase transition.

Laboratory and polaron frames

The Hamiltonian (14) is rather convenient for calculations because it commutes with the excitation operator $N_e = \sigma^+\sigma^- + \sum_k a_k^\dagger a_k$. This allows the use of the standard methods for the study of waveguide QED within the RWA. In the polaron frame the ground state is trivial and the dynamics splits into subspaces of different numbers of excitations. Expected values of observables in the polaron frame are of minor physical relevance, but they are convenient for calculations because the physical observables can be found in terms of them. Since measurements are performed in the laboratory frame, where the Hamiltonian (5) is expressed, it is mandatory to find the relation between both pictures. In what follows, observables with superscript p are observables computed in the polaron frame, i.e.,

$$O^p := \langle\psi^p(t)|O|\psi^p(t)\rangle = \langle\psi(t)U_p^\dagger|O|U_p\psi(t)\rangle, \tag{16}$$

whereas actual observables are given by

$$O = \langle\psi(t)|O|\psi(t)\rangle = \langle\psi^p(t)|U_pOU_p^\dagger|\psi^p(t)\rangle. \tag{17}$$

With this, the dynamics for the atomic excitation, i.e., making $O = \sigma^+\sigma^-$, can be written as

$$P_e = \frac{\Delta_r}{\Delta}\left[P_e^p + 2\,\mathrm{Re}\left(c\sum_k f_k\phi_k^*\right) + 2\sum_{kk'} f_k f_{k'}^*\phi_k^*\phi_{k'}\right] + P_e^{\mathrm{GS}}, \tag{18}$$

where $c = \langle\mathbf{0}|\otimes\langle g|\sigma^-|\psi^p\rangle$ and $\phi_k = \langle\mathbf{0}|\otimes\langle g|a_k|\psi^p\rangle$ are the amplitudes for the excited state and the k-mode field of an arbitrary state in the polaron frame, respectively. The first and last terms of Eq. (18) are the equilibrium, at $T = 0$, atomic populations in the polaron frame and in the ground state, respectively. In fact,

$$P_e^{\mathrm{GS}} = \frac{1}{2}(1 + \langle\sigma^z\rangle_{\mathrm{GS}}) = \frac{1}{2}\left(1 - \frac{\Delta_r}{\Delta}\right), \tag{19}$$

which tells us, among other things, that the ground-state atomic excitation is related to the frequency renormalization Δ_r. We also note that to return to the laboratory framework, both the atomic and field amplitudes are needed. This is a consequence of the nonlocal character of U_p in Eq. (11), which mixes matter and light operators. Finally, we will be interested in the temporal evolution of the occupation of mode n_k. In terms of quantities in the polaron frame, we obtain the relationship

$$n_k(t) = n_k^{\mathrm{GS}} + |\phi_k(t)|^2 - 2\,\mathrm{Re}[c(t)\phi_k(t)f_k]. \tag{20}$$

The same comments as for P_e can be repeated here. Both relations will be used throughout this work.

IV. EQUILIBRIUM PROPERTIES

For sufficiently weak atom-waveguide coupling, the ground state is well approximated by the trivial vacuum $|g\rangle\otimes|\mathbf{0}\rangle$. This is consistent with performing the RWA on (5). A first consequence of entering the USC regime is that strong light-matter correlations are formed. This is easily understood with the polaron *Ansatz*, since the actual ground state (GS) of Eq. (5) can be approximated by

$$\begin{aligned}|\psi_{\mathrm{GS}}\rangle &\cong U_p\,|g\rangle\otimes|\mathbf{0}\rangle\\ &= \frac{1}{\sqrt{2}}\left(|+\rangle\prod_k|-f_k\rangle - |-\rangle\prod_k|f_k\rangle\right),\end{aligned} \tag{21}$$

where $|f_k\rangle = D(f_k)|0_k\rangle$ is a k-mode coherent state, with $D(f_k) = \exp(f_k a_k^\dagger - f_k^* a_k)$ the bosonic displacement operator. States $|\pm\rangle = \frac{1}{\sqrt{2}}(|g\rangle \pm |e\rangle)$ are the atom-symmetric and antisymmetric superpositions, respectively. The state in Eq. (21) is a multiphoton Schrödinger cat state. Its photon number can be obtained via $\langle\psi_{\mathrm{GS}}|a_k^\dagger a_k|\psi_{\mathrm{GS}}\rangle = |f_k|^2$. The photonic profile in position space can be recovered via a discrete Fourier transform

$$f_x = \frac{1}{N_c}\sum_{j,k} f_k e^{ik(x-x_j)}, \tag{22}$$

which indicates that the photonic amplitudes are superpositions of small emitter contributions f_k centered at each coupling point to the waveguide.

The ground state, together with the atomic renormalization frequency Δ_r in Eq. (13), encapsulates the equilibrium properties at zero temperature, in particular, the existence of virtual excitations, both in the atom and in the photonic field, as well as the existence (or absence) of a quantum phase transition. It is known that the spin-boson model undergoes a localization-delocalization transition when $\Delta_r \to 0$ [71]. Again, this transition can also be understood within the polaron formalism. If we look at (14), when $\Delta_r = 0$, the ground state is degenerate, so the gap closes and a quantum phase transition can occur.

A. Atom excitations, renormalization, and the existence of a quantum phase transition

A consequence of light-matter entanglement in the ground state is that the atom is dressed by the quantum fluctuations of waveguide photons. This is reflected in a renormalization of the dressed atomic frequency [see Δ_r in Eqs. (13) and (14)]. Furthermore, using the polaron theory, the qubit excitation probability is given by Eq. (19). Thus, the discussion of Δ_r directly applies to the existence of excitations in the ground state because of the coupling to the waveguide.

In Fig. 2(a) we plot Δ_r as a function of the contact point distance x and the coupling strength α for a giant emitter with $N_c = 3$. Figure 2(b) focuses on particular cases and limits of the renormalization of Δ_r. We have verified that in the limit $x \to 0$ the dipole approximation is recovered, i.e., results must reduce to the case $N_c = 1$. This is a consequence of the normalization used in Eq. (6). For $N_c = 1$, we know that for an Ohmic waveguide, $\Delta_r \sim \Delta(\Delta/\omega_c)^{\alpha/(1-\alpha)}$ in the scaling limit $\Delta/\omega_c \ll 1$ [65], which is shown as a

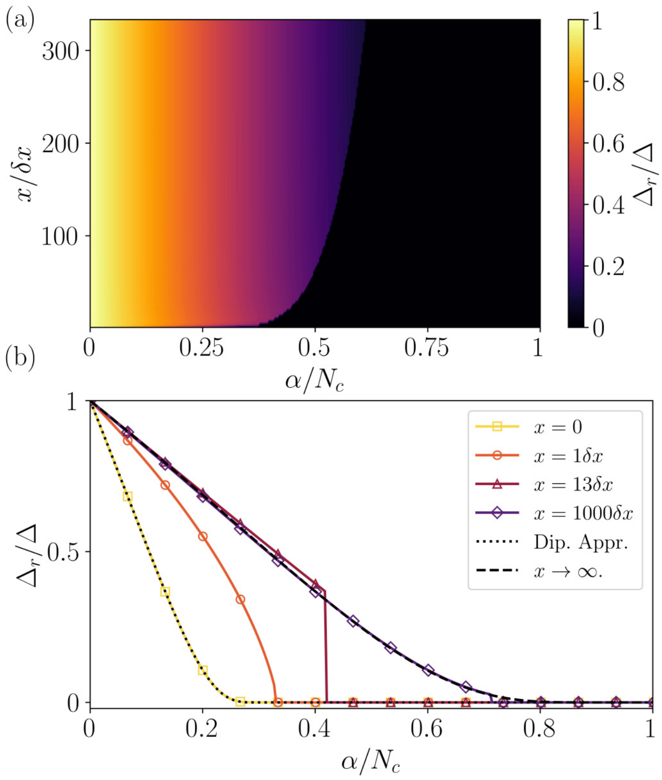

FIG. 2. (a) Renormalization of the two-level system energy with the coupling strength α and the distance between coupling points x for $N_c = 3$. (b) Set of specific values for the distance x between connections showing the phase transition as α increases. For limiting cases we have analytical expressions; for intermediate distances, the transition is more abrupt.

dotted line in Fig. 2(b). On the other hand, when $x \to \infty$, Δ_r behaves as if the contacts points were independent, thus approaching the dipole approximation but with a coupling per contact $\alpha \to \alpha/N_c$ (shaded line), showing perfect agreement with the numerical calculation. An interesting finding is the appearance of a distance-dependent localization transition for a giant emitter, which resembles the one observed for the two-impurity spin-boson model [30,76]. This a consequence of the presence of position-dependent couplings in the giant emitter and the competition between the bare qubit energy and dissipation induced by the Ohmic bath.

The polaron calculations predict a more abrupt decrease of Δ_r, in contrast to the single emitter limit(s). However, it is not clear that our polaron theory is valid in these (intermediate) ranges of coupling, and the results must be contrasted with other approaches. Thus, now we resort to a field-theoretic argument. In fact, the existence of a quantum phase transition in the spin-boson model is well studied in the literature [71,72]. A condition for a symmetry breaking point and thus $\langle\sigma^x\rangle \neq 0$ is that $\int d\omega\, J(\omega)\omega^{-2}$ diverges. This happens whenever $J(\omega) \sim \omega^{1-\beta}$ for $0 < \beta < 1$. The Ohmic case ($N_c = 1$) lies at the margin [75]. It is known that, in this case, there is a continuum transition of the Berezinskii-Kosterlitz-Thouless transition type. This can be proven by mapping the spin-boson model (5) to a gas of charges. Concretely, the partition function can be approximated by [77]

$$Z \sim \exp\left[-4\int_0^\beta d\tau_i \int_0^\beta d\tau_j \epsilon_i\epsilon_j \lambda\left(\frac{\tau_i-\tau_j}{\tau_c}\right)\right], \quad (23)$$

where $\epsilon_i = \pm 1$, $\tau_c = \omega_c^{-1}$ (β^{-1} is the temperature), and the effective interaction is given by

$$\frac{d^2\lambda(\tau)}{d\tau^2} = \omega_c^2 \int d\omega\, J(\omega) e^{-\omega\tau}, \quad (24)$$

which yields $\lambda(\tau) \sim \ln(\tau)$ in the dipole approximation for the Ohmic case, thus a Berezinskii-Kosterlitz-Thouless–like transition. For a giant atom with arbitrary contact points, the integral on the right-hand side can be computed using the general spectral function in Eq. (8) such that

$$\frac{d^2\lambda(\tau)}{d\tau^2} \sim \sum_{j,l}^{N_c} [\tau + i(x_l - x_j)/v_g]^{-2}. \quad (25)$$

As an example, for a giant emitter with $N_c = 3$ equidistant points it yields

$$\lambda(\tau) \sim -3\ln(\tau) - 2\ln(\tau^2 + x^2) - \ln(\tau^2 + 4x^2), \quad (26)$$

i.e., logarithmic interactions persist, one per each leg of the giant emitter, thus confirming the existence of a quantum phase transition in a giant emitter with arbitrary coupling points.

B. Virtual photons in the ground state

The existence of virtual photons around the contact points at ultrastrong coupling has been hypothesized in [22]. Photon localization of the ground state has been successfully studied using polaron and matrix-product-state simulations for a small emitter in [62,73], corroborating the usefulness of the variational polaron *Ansätze*. In this section we describe such photonic clustering for a giant emitter and analyze its spatial profile.

For atoms coupled to cavity-array systems in the USC regime, the photonic cloud generated around the emitter has been found to have an exponentially decaying profile [48,62,73]. Interestingly, the Ohmic model for the waveguide predicts a power-law decay for the photonic cloud localized around each of the contact points of the giant emitter. Furthermore, this power-law decay changes when crossing the quantum phase transition.

Using Eq. (22) and at the scaling limit where $\omega_k \approx v_g|k|$, the virtual photons are given by the Fourier transform of $\sqrt{|k|}/(|k| + \Delta_r/v_g)$. We are interested in the decay of the photonic cloud well away from the connection points, so the corresponding contribution of the integral is that of small-k values. Therefore, there are two limits of the Fourier transform that interest us. Within the delocalized phase $\Delta_r \neq 0$, so we can assume that the contributing k are negligible in front of Δ_r/v_g, leading to a power-law decay with the form $f_x \sim (x - x_j)^{-3/2}$. Instead, after crossing the quantum phase transition to the localized regime $\Delta_r = 0$ and the decay goes as $f_x \sim (x - x_j)^{-1/2}$.

In Fig. 3 we plot an example of the ground-state photons in real space $\langle\psi_{GS}|a_x^\dagger a_x|\psi_{GS}\rangle = |f_x|^2$ for both cases, with $N_c = 5$ and $x = 20\delta x$. Figure 3(a) illustrates the case for $\Delta_r \neq 0$. We observe sharp peaks around each of the coupling points

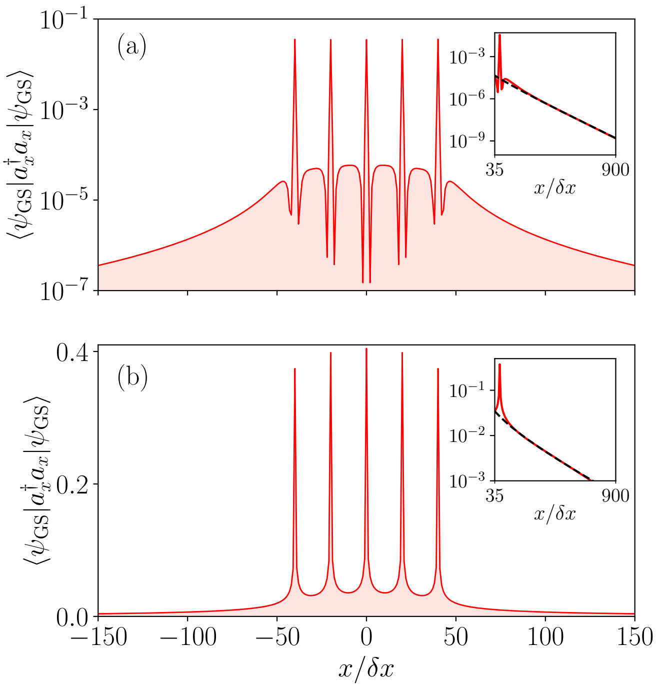

FIG. 3. (a) Ground-state photons for a giant atom with five connection points ($N_c = 5$) with coupling strength $\alpha/N_c = 1/5$, in this case $\Delta_r \neq 0$. The inset focuses on the profile of the photonic clouds around the rightmost coupling point. A fitting into a power-law decay x^{-a}, plotted as a black dashed line, leads to the exponent $a \simeq 2.96$. (b) Ground-state photons for $\alpha/N_c = 2/5$, corresponding to $\Delta_r = 0$. The decay also fits into a power law, in this case with $a \simeq 1.09$. For both plots, the distance between the closest couplings is $x = 20\delta x$, the cutoff frequency is $\omega_c = 3$, $\Delta = 1$, and the number of modes $N = 15\,001$.

and each of these peaks is surrounded by abrupt dips and a slowly decaying profile. The dips can be attributed to the overlap between the sharp peaks and slow decays. For this case we predict a power-law decay of the photonic profile away from the emitter scaling as approximately x^{-3}. The inset of the figure is a close-up of the rightmost coupling point and shows a power-law fit by a black shaded line. From the fit we recover a decay approximately equal to $x^{-2.96}$, which agrees with our prediction. The other example shown in Fig. 3(b) corresponds to $\Delta_r = 0$. Here the peaks become higher and sharper, the dips disappear, and the decay becomes slower. Again, fitting the profile away from the rightmost coupling point, we have a power-law decay approximately equal to $x^{-1.09}$, which perfectly agrees with our analytical estimation.

V. RELAXATION RATE AND LAMB SHIFT

In the simplest approach, the spontaneous emission of an emitter in a continuum is obtained by means of Fermi's golden rule. Using second-order perturbation theory (in the light-matter coupling) a two-level system with level splitting Δ decays with a rate $\gamma = J(\Delta)$. Also, the atom frequency is dressed by the Lamb shift δ.

Interestingly, for a giant emitter with multiple contact points, interference effects start to play an important role in the relaxation dynamics. The fact that the emitter-waveguide interaction is no longer local introduces a new timescale in the system accounting for the time delay between different coupling points $\zeta = x/v_g$. When this time delay is much smaller than the excited-state lifetime of the system as if it had a single coupling point $\zeta \ll J_{\rm Ohm}(\Delta)^{-1}$, memory effects can be neglected [11,22]. Consequently, an effective relaxation rate γ_r and the frequency shift can be obtained in this regime by using the Fermi golden rule, which now depends on the distance between coupling points and can be engineered to suppress or enhance spontaneous emission.

In the USC regime, both the emission rates and Lamb shift can be calculated in a similar way as in the perturbative regime. The only difference is that the formulas are now evaluated at the renormalized frequency Δ_r instead of the bare one Δ [cf. Eq. (13)] [65,66]. Then

$$\gamma_r = J(\Delta_r) = J_{\rm Ohm}(\Delta_r)G(\Delta_r) \tag{27}$$

and

$$\delta = \frac{2\Delta_r^2}{\pi} P \int_0^\infty d\omega \frac{J(\omega)}{(\Delta_r - \omega)(\omega + \Delta_r)^2}, \tag{28}$$

where P denotes the principal value. In Fig. 4(a) we show the normalized relaxation rate as a function of the distance $x/\delta x$ between contact points, for two values of the coupling parameter: $\alpha = 0.01$, where we recover the weak coupling or RWA results [11,22], and $\alpha = 0.16$, where the RWA breaks down.

We observe that increasing the emitter-waveguide coupling beyond the RWA produces a shift in position for the relaxation rate, displacing characteristic points of destructive and constructive interference. This shift is a consequence of the renormalization of the giant emitter frequency and it has to be taken into account in order to observe interference effects in experiments with ultrastrongly coupled giant emitters.

The Lamb shift, plotted in Fig. 4(b) reflects the same shift in position as the relaxation rate. A more complete image of this behavior is given in Fig. 4(c), where the shift is limited by the localization transition appearing at larger values of the coupling (deep strong coupling). Therefore, the spontaneous decay in a giant emitter is strongly affected by interference between contact points. This behavior persists in the USC regime but with values that become strongly modified as the coupling α increases.

VI. EMITTER AND FIELD DYNAMICS

The effective number-preserving Hamiltonian (14) permits us to work in the single-excitation sector and apply standard RWA methods. Using the dynamical polaron *Ansatz*, the time-dependent state vector in the polaron frame can be described as [65]

$$|\psi^P(t)\rangle = c(t)|e\rangle|\mathbf{0}\rangle + \sum_k \phi_k(t)|g\rangle a_k^\dagger|\mathbf{0}\rangle. \tag{29}$$

The amplitudes of the polaron state vector satisfy the set of dynamical equations

$$i\dot{\tilde{c}} = 2\Delta_r \sum_k f_k \tilde{\phi}_k e^{-i(\omega_k - \Delta_r)t}, \tag{30a}$$

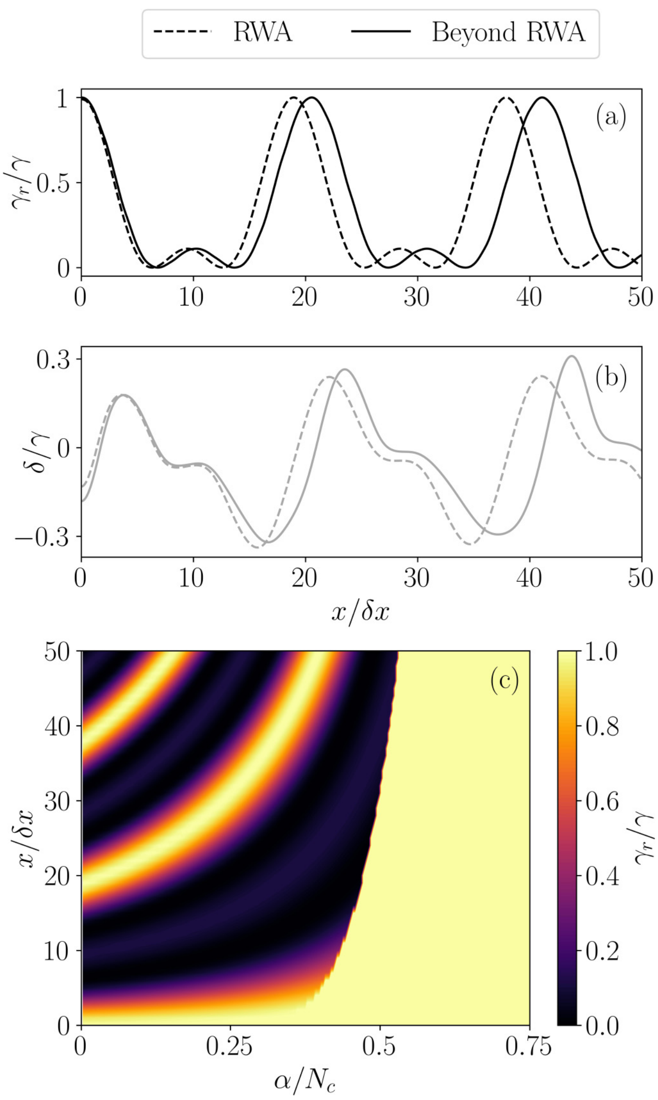

FIG. 4. (a) Normalized effective decay rate and (b) Lamb shift for a giant emitter with three coupling points ($N_c = 3$) and bare qubit frequency $\Delta = 1$ as a function of the spacing between connections. Dashed lines indicate the behavior for $\alpha = 0.01$ (RWA) and solid lines $\alpha = 0.16$ (beyond the RWA). (c) Full dependence of the effective decay rate on the coupling strength and the distance between coupling points.

$$i\dot{\tilde{\phi}}_k = 2\Delta_r f_k \left(\tilde{c} e^{i(\omega_k - \Delta_r)t} + \sum_l f_l \tilde{\phi}_l \right), \tag{30b}$$

where we have shifted to different rotating frames $\tilde{c} = e^{i\Delta_r t/2} c$ and $\tilde{\phi}_k = e^{i(\omega_k - \Delta_r/2)t}\phi_k$ in order to simplify the equations. Equations (30a) and (30b) can be integrated numerically, obtaining any observable in the polaron frame. Then, by using the relation (18) or (20), the observables in the laboratory frame can be computed.

Before looking at the numerical results, it is convenient to discuss some generalities about the expected dynamical behavior. For this we can neglect the contributions of the V_{local} operator, which only produces a photon frequency shift that does not significantly contribute to the single-excitation dynamics. In addition, it makes further analytical treatment

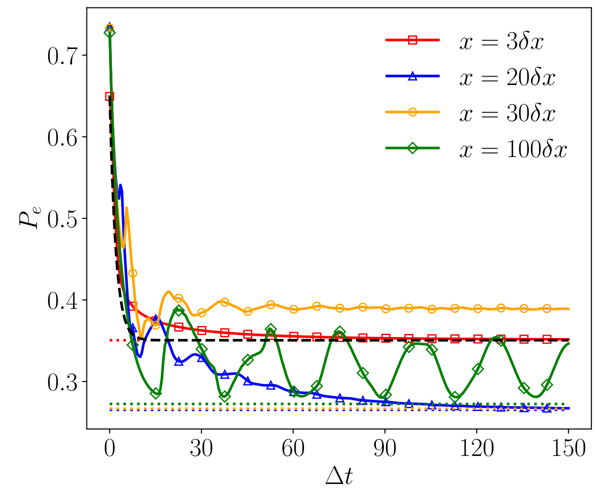

FIG. 5. Evolution of the excited-state probability of a giant emitter with three coupling points $N_c = 3$ for three different distances between contact points and fixed coupling strength $\alpha = 0.8$, $\Delta = 1$, $\omega_c = 6$, and $N = 3000$. The expected equilibrium probabilities P_e^{GS} are illustrated with horizontal dotted lines.

difficult and it is not relevant for the results discussed in this section. If this is done, the set of equations is formally equivalent to the one-excitation dynamics in RWA models and the Wigner-Weisskopf theory can be directly applied. Integrating out the photonic degrees of freedom, a (nonlocal) differential equation for $\tilde{c}(t)$ is obtained,

$$\dot{\tilde{c}} = -\frac{2\Delta_r^2}{\pi} \int_0^\infty \frac{J(\omega)d\omega}{(\omega + \Delta_r)^2} \int_0^t d\tau\, \tilde{c}(t-\tau) e^{i(\omega - \Delta_r)\tau}. \tag{31}$$

The dependence of the spectral function on the time delays between coupling points ζ gives rise to a multiple-time-delay differential equation for the excited-state amplitude,

$$\dot{\tilde{c}}(t) = -\frac{\gamma}{2N_c^2} \sum_{j=0}^{N_c-1} (N_c - j) e^{i\Delta_r j\zeta} \tilde{c}(t - j\zeta)\Theta(t - j\zeta). \tag{32}$$

Here $\Theta(\cdot)$ is the Heaviside step function. The time delays $j\zeta$ introduce new timescales in the system and non-Markovian effects are expected.

An analogous time-delay equation was first presented in [17] within the RWA regime for the same continuous model studied here. These types of non-Markovian dynamical equations have also been found in the study of the spontaneous emission in single-end optical fibers [28], atoms in front of reflecting mirrors [26], and two distant emitters in waveguide QED, within the RWA [29] and beyond the RWA [30]. In particular, in addition to the relaxation rate previously discussed, oscillations in the emitter dynamics will occur.

On top of that, already in the RWA regime the existence of bound states for giant atoms has been discussed [17]. These can exist even in the absence of band gaps as an interference effect, as seen in Fig. 5, due to the spatial separation of coupling points. Bound states arising from interference effects are also present in the USC regime, as we will show later in numerical simulations.

Applying a Laplace transform in Eq. (32) gives us insight into the nature of these bound states. By defining the excited-state amplitude in Laplace space as $\hat{c}(s) = \int_0^\infty dt\, e^{-st}\tilde{c}(t)$ we have

$$\hat{c}(s) = \left[s + \frac{i\Delta_r}{2} + \frac{\gamma}{2N_c^2}\sum_{j=0}^{Nc-1}(N_c - j)e^{(-s+i\Delta_r/2)j|\zeta|}\right]^{-1}, \tag{33}$$

where we have set $\tilde{c}(0) = 1$ in order to study the spontaneous emission. The above dynamical equation in the Laplace space is exactly the same as that obtained for the RWA limit in [17], with the difference that the bare qubit frequency Δ must be replaced by Δ_r.

By definition, bound states do not radiate; thus (if they exist) they are purely imaginary poles of Eq. (33). Searching for purely imaginary poles with the form $s_n = -i2n\pi/N_c\zeta$, with $n \in \mathbb{N}$, we obtain

$$\Delta_r\zeta = \frac{2n\pi}{N_c} - \frac{J_{\rm Ohm}(\Delta_r)\zeta}{2N_c}\cot\left(\frac{n\pi}{N_c}\right), \tag{34}$$

where $\zeta = x/v_g$ is the time delay between the two closest coupling points. It is worth recalling that all these relations neglect the local $V_{\rm local}$ operator [cf. the Hamiltonian (14)]. They are however a good estimation for understanding the emitter dynamics and locating the appearance of bound states in the parameter space of the model, in particular, that their existence requires a finite time delay ζ and that the renormalized atom frequency and spontaneous emission play a role.

The existence of both bound states and non-Markovian dynamics in the USC regime can be proven by monitoring the spontaneous emission. In doing so we assume the atom waveguide at the GS and then the qubit is driven within a π pulse. After the pulse the wave function is given by $|\psi(0)\rangle = \sigma^+|\mathrm{GS}\rangle$. Since $[\sigma^x, U_p] = 0$, we may work in the single-excitation manifold in the polaron picture. Therefore, we can numerically integrate Eqs. (30a) and (30b), including the $V_{\rm local}$ terms, and transform back to the laboratory frame using Eq. (18). In Fig. 5 we plot the spontaneous emission. We notice that $P_e(t=0) \neq 1$, since for our initial state $P_e = 1/2(1 + \Delta_r/\Delta)$ [cf. Eq. (18)]. Furthermore, each of the plotted decay processes has a different equilibrium excited-state occupancy, as given by Eq. (19). As shown in Fig. 5 for $x = 3\delta x$, short time delays between coupling points lead to relaxations that can be closely described by an exponential decay defined by the effective spontaneous emission rate in Eq. (27). The evolution of the excited-state occupancy can be well approximated by

$$P_e \approx P_e^{\rm GS} + \frac{\Delta_r}{\Delta}e^{-\gamma_r t}, \tag{35}$$

plotted by the black dashed line in Fig. 5. The lack of major non-Markovian effects can be seen via Eq. (33), as the limit $\zeta \to 0$ leads to a time evolution governed by the decay rate γ_r.

For a sufficiently large distance between coupling points, non-Markovianity takes a central role, as illustrated by the decay for $x = 20\delta x$ in Fig. 5. Initially, it has an approximately exponential decay given by $J_{\rm Ohm}(\Delta_r)$, until the emitted light reaches a coupling point. Then an oscillatory behavior increases as the light emitted from one connection point is partially reabsorbed and emitted back to the waveguide by another contact point. At longer times, these oscillations become damped as the energy is gradually emitted outside the atom, until the system reaches equilibrium at the corresponding $P_e^{\rm GS}$.

We encounter a different behavior for $x = 30\delta x$ in Fig. 5. Due to the interference of the field emitted from each coupling point, the system relaxes to a bound state, as signaled by the difference in occupancy from the ground state once the evolution reaches the equilibrium. This comes as a direct consequence of the initial excited state having a nonzero overlap with bound states for these parameters.

Furthermore, Fig. 5 illustrates yet another type of decay. For $x = 100\delta x$ we find long-lived oscillations around an equilibrium value higher than $P_e^{\rm GS}$. This is reminiscent of the reported oscillating bound states in the RWA [17]. In the next section we discuss how these oscillating bound states behave whenever the coupling cannot be treated perturbatively.

Oscillating bound states

Some interest has been aroused in the existence of oscillating bound states [17,69]. They originate from the interplay of two coexisting bound states. Consequently, part of the field emitted during the spontaneous emission process is trapped while oscillating between the coupling points of the emitter. In USC, approximate oscillating bound states are found by searching for two coexisting solutions of Eq. (34). Due to the dependence of Δ_r on α and ζ, via the variational parameters f_k, the existence of two solutions for the same set of parameters cannot be analytically proven. This numerically requires fine-tuning, which at most allows for the prediction of oscillating bound states with large but finite lifetime in USC, as illustrated in Fig. 5 for $x = 100\delta x$.

Figure 6(a) illustrates the excited-state population P_e of a giant atom with increasing coupling strength α. The rest of the parameters are set so that in the RWA regime the excited state decays into an oscillating bound state. It is clear that the oscillating bound state found for the lower couplings is lost as α increases. Figure 6(b) focuses on two specific values of the coupling strength showing the long time behavior of the oscillating bound state and its counterpart at higher coupling, for which the population revivals slowly decrease in amplitude. The field evolutions corresponding to both cases are plotted in Figs. 6(c) and 6(d), respectively.

Within the RWA, fixing the distance between coupling points and increasing the coupling should eventually reach another pair of simultaneous solutions for Eq. (34) and therefore an oscillating bound state [17]. In contrast, our simulations indicate that entering the USC regime leads to the loss of the oscillating bound state due to the renormalization of Δ_r and eventually to the quantum phase transition. This same trend has also been recently reported in [69], where matrix-product-state simulations showed this same breakdown of the periodicity for the existence of oscillating bound states in parameter space with the coupling strength.

VII. SUMMARY AND CONCLUSIONS

In this work we have developed a semianalytical approach for the low-energy sector of giant emitters in the ultrastrong

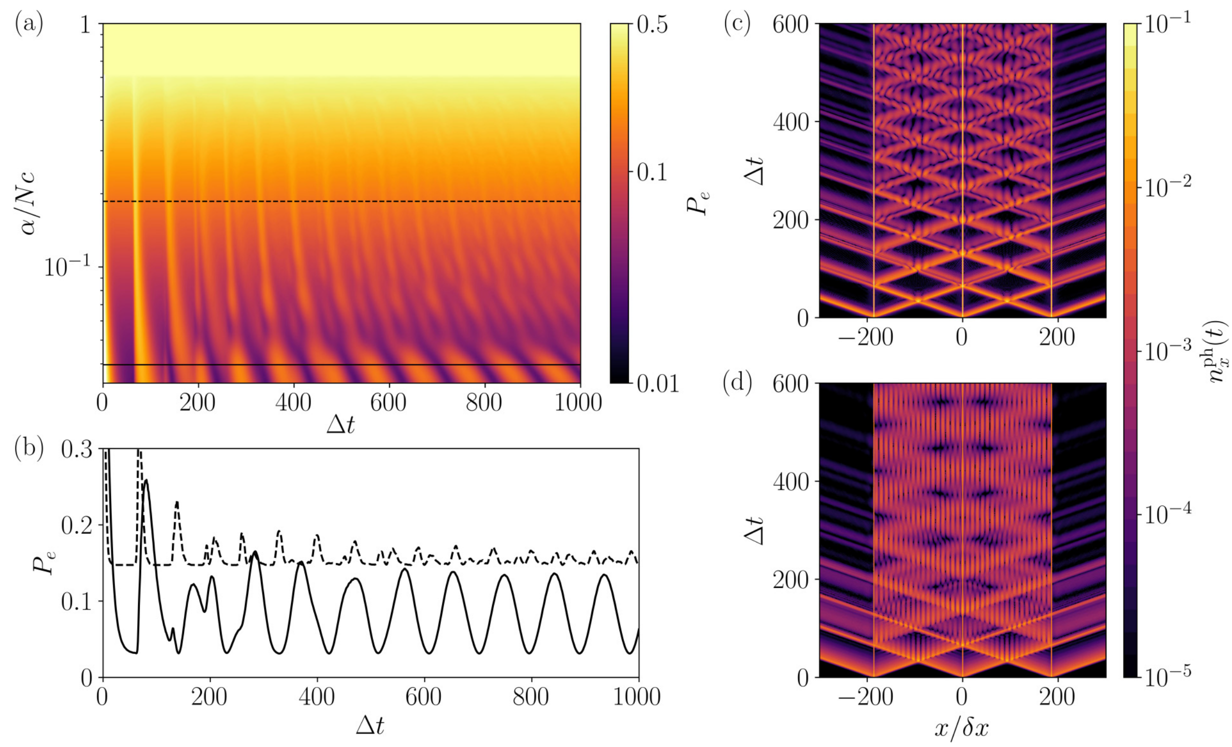

FIG. 6. (a) Time evolution of the excited-state population P_e with increasing coupling α. Black horizontal lines point to the two cases highlighted in the other plots of the figure. (b) Plot of the spontaneous emission into an oscillating bound state in the RWA for $\alpha \simeq 0.118$ (solid line) and for an increased coupling of $\alpha \simeq 0.557$, within the USC (dashed line). The field emitted into the waveguide for these cases is plotted in (d) and (c), respectively. These simulations are carried out for a giant atom with three connections $N_c = 3$ with the parameters $\zeta = 186\delta x$, $\omega_c = 3$, $\Delta = 1$, and number of modes $N = 4001$.

regime based on polaronlike methods. In particular, we have focused on a single giant atom coupled via N_c connection points to an Ohmic waveguide.

We have characterized the ground state of the system. In particular, we have analyzed the virtual photons surrounding each of the coupling points. The latter decays spatially away from the connection points to the waveguide as a power law, unlike what occurs for pointlike emitters in a cavity array [73]. We also have studied the renormalization of the atomic frequency Δ_r and shown that the system exhibits a localization-delocalization quantum phase transition which is dependent not only on the coupling strength α but also on the distance between coupling points.

For the dynamics of the system we have focused on the spontaneous emission. We have derived analytical expressions for the Lamb shift δ and effective decay rate γ_r which characterize the early evolution of the system whenever its lifetime is much larger than the time delay $\zeta = x/v_g$ between coupling points. Both of these values were reported to have a periodic behavior with the distance between coupling points in the RWA regime [11]. We find that this periodicity is lost in USC due to the renormalization of Δ_r. These results suggest that in real implementations of waveguide QED with giant atoms that require going beyond the RWA, most of the predicted non-Markovian effects might be blurred by the renormalization of the bare atom. We were able to fully characterize the dynamics within the polaron frame, providing an approximate analytical expression for the evolution of the excited-state amplitude. We find that some of the non-Markovian dynamics found in the RWA, such as the nonexponential decay [7] and bound states arising from the interference of the spontaneous emission from different coupling points [17], still hold in the USC regime. However, other behaviors, such as the recurrence of oscillating bound states as the coupling increases [17], are lost when entering the USC regime. Instead, as the localization-delocalization transition is approached by increasing the coupling strength α, the oscillations in the excited-state occupancy have a sharp drop in amplitude, becoming irregular in time and eventually disappear.

ACKNOWLEDGMENTS

The authors acknowledge funding from the EU (COST Action 15128 MOLSPIN, QUANTERA SUMO, and FET-OPEN Grant No. 862893 FATMOLS), the Spanish Government Grants No. MAT2017-88358-C3-1-R and No. PID2020-115221GB-C41/AEI/10.13039/501100011033, the Gobierno de Aragón (Grant No. E09-17R Q-MAD), and the CSIC Quantum Technologies Platform PTI-001. C.A.G.-G. acknowledges funding from the program Acciones de Dinamización “Europa Excelencia” Grant No. EUR2019-103823. F.N. was supported in part by Nippon Telegraph and Telephone Corporation Research, the Japan Science and Technology Agency (via the Quantum Leap Flagship Program and the Moonshot R&D Grant No. JPMJMS2061), the Japan Society for the Promotion of Science (via the Grants-in-Aid for Scientific Research Grant No. JP20H00134), the Army Research Office (Grant No. W911NF-18-1-0358), the Asian Office of Aerospace Research and Development (via Grant No. FA2386-20-1-4069), and the Foundational Questions Institute Fund via Grant No. FQXi-IAF19-06.

APPENDIX A: DERIVATION OF THE SPIN-BOSON HAMILTONIAN

In this Appendix we find the Hamiltonian describing the system represented in Fig. 1(b), which leads to the spin-boson form given in Eq. (5). As mentioned in Sec. II, we model the waveguide as an one-dimensional chain of N inductively coupled LC resonators with equal inductances L_0 and capacitances C_0. The Lagrangian for such a system is

$$\mathcal{L}_{\rm wg} = \sum_{n=1}^{N} \frac{(\phi_n - \phi_{n+1})^2}{2L_0} + \frac{C_0\dot{\phi}_n^2}{2}. \tag{A1}$$

The waveguide Hamiltonian can be obtained via a Legendre transform

$$H_{\rm wg} = \sum_{n=1}^{N} \frac{(\phi_n - \phi_{n+1})^2}{2L_0} + \frac{Q_n^2}{2C_0}, \tag{A2}$$

where $Q_n = \partial\mathcal{L}_{\rm wg}/\partial\dot{\phi}_n$ are the charges of each LC resonator.

Assuming periodic boundary conditions, the Hamiltonian (A2) can be diagonalized by means of a Fourier transform $\phi_k = 1/\sqrt{N}\sum_k \phi_n e^{ikx_n}$,

$$H_{\rm wg} = \sum_k \frac{|Q_k|^2}{2C_0} + [2 - 2\cos(k\delta x)]\frac{|\phi_k|^2}{2L_0}, \tag{A3}$$

where $k = 2\pi n/L$, $L = N\delta x$, and δx is the size of an LC resonator. From Eq. (A3) we obtain the dispersion relation in Eq. (3).

After quantization of the field, the waveguide is described as

$$H_{\rm wg} = \sum_k \omega_k\left(a_k^\dagger a_k + \frac{1}{2}\right). \tag{A4}$$

We model our qubit as a transmon [78]. Because of the capacitive coupling of the N_c coupling points to the qubit, the Hamiltonian is given by

$$\begin{aligned} H =& \frac{1}{2(C_g + C_J)}\left(Q_q + \sum_j C_g V(x_j)\right)^2 \\ &- E_J\cos(2\pi\phi_q/\Phi_0) + H_{\rm wg}. \end{aligned}\tag{A5}$$

At this point we assume that all terms of the order $[C_g/(C_g + C_J)]^2$ are negligible as $C_J \gg C_g$, which leads to the Hamiltonian

$$\begin{aligned} H =& \frac{Q_q^2}{2(C_g + C_J)} - E_J\cos(2\pi\phi_q/\Phi_0) \\ &+ \sum_j C_g Q_q V(x_j) + H_{\rm wg}. \end{aligned}\tag{A6}$$

The voltage within the waveguide is given by

$$\begin{aligned} V(x_j) &= \partial_t\phi_j = i[H_{\rm wg}, \phi_j] \\ &= \sum_{j=1}^{N_c} C_g Q_q \sum_k \sqrt{\frac{\omega_k}{2L}}(a_k e^{ikx_j} + a_k^\dagger e^{-ikx_j}). \end{aligned}\tag{A7}$$

By truncating the qubit subsystem to its first two levels we arrive at

$$\begin{aligned} H =& \frac{\Delta}{2}\sigma_z + \sum_k \omega_k\left(a_k^\dagger a_k + \frac{1}{2}\right) \\ &+ C_g\sigma_x \sum_j^{N_c}\sum_k \sqrt{\frac{\omega_k}{2L}}(a_k e^{ikx_j} + a_k^\dagger e^{-ikx_j}). \end{aligned}\tag{A8}$$

yielding the spin-boson model in Eq. (5).

APPENDIX B: POLARON TRANSFORMATION

In this Appendix we detail the main aspects of the polaron transformation defined in Eq. (11). In particular, we show how to find its variational parameters, as given in Eq. (12), and the atomic frequency renormalization given by Eq. (13). We also derive the expressions in the laboratory frame used in the main text [Eqs. (18)–(20)].

The unitary transformation (11) contains the variational parameters f_k that are found minimizing the energy functional. On top of that, the basic idea is that U_p disentangles the two-level system from the waveguide. Thus, in the polaron picture, H_p conserves the number of excitations and becomes tractable with the same techniques as RWA models; in particular, we can compute the single-excitation eigenstates. It is interesting to note that the GS obtained from the variational method is an eigenstate of H_p. This serves as a consistency test confirming that the effective RWA model is accurate: If the GS is well represented, the lowest-lying excitations are single-particle excitations over it.

It is convenient to see how different operators transform under U_p. For example,

$$U_p^\dagger a_k U_p = a_k - f_k\sigma_x \tag{B1}$$

and

$$\begin{aligned} U_p^\dagger\sigma_z U_p &= \exp\left(2\sigma_x\sum_k(f_k a_k^\dagger - f_k a_k)\right)\sigma_z \\ &= \exp\left(-2\sum_k|f_k|^2\right)\exp\left(2\sigma_x\sum_k f_k a_k^\dagger\right) \\ &\quad\times\exp\left(-2\sigma_x\sum_k f_k a_k\right)\sigma_z. \end{aligned}\tag{B2}$$

By expanding the operators in Eq. (B2) and retaining terms up to second order in f_k we arrive at

$$\begin{aligned} U_p^\dagger\sigma_z U_p \approx& \exp\left(-2\sum_k|f_k|^2\right)\left(1 + 2\sigma_x\sum_k f_k(a_k^\dagger - a_k)\right. \\ &\left.-4\sum_{k,p} f_k f_p a_k^\dagger a_p\right)\sigma_z. \end{aligned}\tag{B3}$$

Then the transformed Hamiltonian H_p can be written as

$$\begin{aligned} H_p = {} & \frac{\Delta_r}{2}\sigma_z + \sum_k \omega_k a_k^\dagger a_k + \sum_k g_k(a_k + a_k^\dagger)\sigma_x \\ & + \Delta_r \sum_k f_k(a_k^\dagger - a_k)\sigma_x\sigma_z - 2\Delta_r \sum_{k,p} f_k f_p a_k^\dagger a_p \sigma_z \\ & - \sum_k f_k\omega_k(a_k^\dagger - a_k)\sigma_x + \sum_k \omega_k |f_k|^2 - 2\sum_k g_k f_k, \end{aligned} \tag{B4}$$

where Δ_r is defined as in Eq. (13). The ground-state energy of this system is given by $E_{\rm ZP}$ in Eq. (15). By minimizing this quantity in terms of the variational parameters $\partial_{f_k} E_{\rm ZP} = 0$, we find the optimal variational parameters [Eq. (12)]. Finally, the effective Hamiltonian in Eq. (14) follows after introducing the expression in Eq. (12) for the variational parameters in Eq. (B4) and using $\sigma_x \mp \sigma_x\sigma_z = 2\sigma^\pm$.

Expectation values in the polaron picture

Expectation values in the laboratory frame of qubit and waveguide mode occupancies can be found using Eqs. (B3) and (B1), respectively. For the excited-state probability we have

$$\begin{aligned} P_e &= \tfrac{1}{2}(1 + \langle\sigma^z\rangle) = \tfrac{1}{2}(1 + \langle\psi|\sigma_z|\psi\rangle) \\ &= \tfrac{1}{2}(1 + \langle\psi^p|U_p\sigma_z U_p^\dagger|\psi^p\rangle), \end{aligned} \tag{B5}$$

where $|\psi^p\rangle$ is the state vector of interest, in the one-excitation subspace given by Eq. (29) yielding Eq. (18).

Similarly, the expectation value n_k in the laboratory frame is given by

$$\begin{aligned} n_k &= \langle\psi|a_k^\dagger a_k|\psi\rangle = \langle\psi^p|U_p a_k^\dagger a_k U_p^\dagger|\psi^p\rangle \\ &= \langle\psi^p|a_k^\dagger a_k - f_k(a_k^\dagger - a_k)\sigma_x + |f_k|^2|\psi^p\rangle. \end{aligned} \tag{B6}$$

Again, using Eq. (29), we obtain Eq. (20), where $n_k^{\rm GS} = |f_k|^2$.

[1] V. Weisskopf and E. Wigner, Berechnung der natürlichen linienbreite auf grund der diracschen lichttheorie, Z. Phys. **63**, 54 (1930).

[2] D. Roy, C. M. Wilson, and O. Firstenberg, *Colloquium*: Strongly interacting photons in one-dimensional continuum, Rev. Mod. Phys. **89**, 021001 (2017).

[3] A. S. Sheremet, M. I. Petrov, I. V. Iorsh, A. V. Poshakinskiy, and A. N. Poddubny, Waveguide quantum electrodynamics: Collective radiance and photon-photon correlations, arXiv:2103.06824 [Rev. Mod. Phys. (to be published)].

[4] T. Li, A. Miranowicz, X. Hu, K. Xia, and F. Nori, Quantum memory and gates using a Λ-type quantum emitter coupled to a chiral waveguide, Phys. Rev. A **97**, 062318 (2018).

[5] M. V. Gustafsson, T. Aref, A. F. Kockum, M. K. Ekström, G. Johansson, and P. Delsing, Propagating phonons coupled to an artificial atom, Science **346**, 207 (2014).

[6] G. Andersson, B. Suri, L. Guo, T. Aref, and P. Delsing, Non-exponential decay of a giant artificial atom, Nat. Phys. **15**, 1123 (2019).

[7] L. Guo, A. Grimsmo, A. F. Kockum, M. Pletyukhov, and G. Johansson, Giant acoustic atom: A single quantum system with a deterministic time delay, Phys. Rev. A **95**, 053821 (2017).

[8] S. Longhi, Photonic simulation of giant atom decay, Opt. Lett. **45**, 3017 (2020).

[9] Q.-Y. Qiu, Y. Wu, and X.-Y. Lü, Collective radiance of giant atoms in non-Markovian regime, arXiv:2205.10982.

[10] X.-L. Yin, W.-B. Luo, and J.-Q. Liao, Non-Markovian disentanglement dynamics in double-giant-atom waveguide-QED systems, Phys. Rev. A **106**, 063703 (2022).

[11] A. Frisk Kockum, P. Delsing, and G. Johansson, Designing frequency-dependent relaxation rates and Lamb shifts for a giant artificial atom, Phys. Rev. A **90**, 013837 (2014).

[12] A. F. Kockum, G. Johansson, and F. Nori, Decoherence-Free Interaction between Giant Atoms in Waveguide Quantum Electrodynamics, Phys. Rev. Lett. **120**, 140404 (2018).

[13] B. Kannan, M. J. Ruckriegel, D. L. Campbell, A. F. Kockum, J. Braumüller, D. K. Kim, M. Kjaergaard, P. Krantz, A. Melville, B. M. Niedzielski, A. Vepsäläinen, R. Winik, J. L. Yoder, F. Nori, T. P. Orlando, S. Gustavsson, and W. D. Oliver, Waveguide quantum electrodynamics with superconducting artificial giant atoms, Nature (London) **583**, 775 (2020).

[14] L. Du, Y.-T. Chen, Y. Zhang, and Y. Li, Giant atoms with time-dependent couplings, Phys. Rev. Res. **4**, 023198 (2022).

[15] A. Soro, C. S. Muñoz, and A. F. Kockum, Interaction between giant atoms in a one-dimensional structured environment, arXiv:2208.04102.

[16] A. M. Vadiraj, A. Ask, T. G. McConkey, I. Nsanzineza, C. W. S. Chang, A. F. Kockum, and C. M. Wilson, Engineering the level structure of a giant artificial atom in waveguide quantum electrodynamics, Phys. Rev. A **103**, 023710 (2021).

[17] L. Guo, A. F. Kockum, F. Marquardt, and G. Johansson, Oscillating bound states for a giant atom, Phys. Rev. Res. **2**, 043014 (2020).

[18] S. Guo, Y. Wang, T. Purdy, and J. Taylor, Beyond spontaneous emission: Giant atom bounded in the continuum, Phys. Rev. A **102**, 033706 (2020).

[19] X. Wang, T. Liu, A. F. Kockum, H.-R. Li, and F. Nori, Tunable Chiral Bound States with Giant Atoms, Phys. Rev. Lett. **126**, 043602 (2021).

[20] W. Zhao and Z. Wang, Single-photon scattering and bound states in an atom-waveguide system with two or multiple coupling points, Phys. Rev. A **101**, 053855 (2020).

[21] L. Du, M.-R. Cai, J.-H. Wu, Z. Wang, and Y. Li, Single-photon nonreciprocal excitation transfer with non-Markovian retarded effects, Phys. Rev. A **103**, 053701 (2021).

[22] A. F. Kockum, in *International Symposium on Mathematics, Quantum Theory, and Cryptography*, edited by T. Takagi, M. Wakayama, K. Tanaka, N. Kunihiro, K. Kimoto, and Y. Ikematsu (Springer Singapore, Singapore, 2021), pp. 125–146.

[23] N. Vats and S. John, Non-Markovian quantum fluctuations and superradiance near a photonic band edge, Phys. Rev. A **58**, 4168 (1998).

[24] H.-P. Breuer and F. Petruccione, *The Theory of Open Quantum Systems* (Oxford University Press, Oxford, 2007).

[25] I. de Vega and D. Alonso, Dynamics of non-Markovian open quantum systems, Rev. Mod. Phys. **89**, 015001 (2017).
[26] U. Dorner and P. Zoller, Laser-driven atoms in half-cavities, Phys. Rev. A **66**, 023816 (2002).
[27] H. Pichler and P. Zoller, Photonic Circuits with Time Delays and Quantum Feedback, Phys. Rev. Lett. **116**, 093601 (2016).
[28] T. Tufarelli, F. Ciccarello, and M. S. Kim, Dynamics of spontaneous emission in a single-end photonic waveguide, Phys. Rev. A **87**, 013820 (2013).
[29] K. Sinha, A. González-Tudela, Y. Lu, and P. Solano, Collective radiation from distant emitters, Phys. Rev. A **102**, 043718 (2020).
[30] C. A. González-Gutiérrez, J. Román-Roche, and D. Zueco, Distant emitters in ultrastrong waveguide QED: Ground-state properties and non-Markovian dynamics, Phys. Rev. A **104**, 053701 (2021).
[31] S. Arranz Regidor, G. Crowder, H. Carmichael, and S. Hughes, Modeling quantum light-matter interactions in waveguide QED with retardation, nonlinear interactions, and a time-delayed feedback: Matrix product states versus a space-discretized waveguide model, Phys. Rev. Res. **3**, 023030 (2021).
[32] S. Arranz Regidor and S. Hughes, Cavitylike strong coupling in macroscopic waveguide QED using three coupled qubits in the deep non-Markovian regime, Phys. Rev. A **104**, L031701 (2021).
[33] P. Y. Wen, K.-T. Lin, A. F. Kockum, B. Suri, H. Ian, J. C. Chen, S. Y. Mao, C. C. Chiu, P. Delsing, F. Nori, G.-D. Lin, and I.-C. Hoi, Large Collective Lamb Shift of Two Distant Superconducting Artificial Atoms, Phys. Rev. Lett. **123**, 233602 (2019).
[34] T. Niemczyk, F. Deppe, H. Huebl, E. P. Menzel, F. Hocke, M. J. Schwarz, J. J. Garcia-Ripoll, D. Zueco, T. Hümmer, E. Solano, A. Marx, and R. Gross, Circuit quantum electrodynamics in the ultrastrong-coupling regime, Nat. Phys. **6**, 772 (2010).
[35] P. Forn-Díaz, J. Lisenfeld, D. Marcos, J. J. García-Ripoll, E. Solano, C. J. P. M. Harmans, and J. E. Mooij, Observation of the Bloch-Siegert Shift in a Qubit-Oscillator System in the Ultrastrong Coupling Regime, Phys. Rev. Lett. **105**, 237001 (2010).
[36] F. Yoshihara, T. Fuse, S. Ashhab, K. Kakuyanagi, S. Saito, and K. Semba, Superconducting qubit-oscillator circuit beyond the ultrastrong-coupling regime, Nat. Phys. **13**, 44 (2017).
[37] P. Forn-Díaz, J. García-Ripoll, B. Peropadre, J.-L. Orgiazzi, M. Yurtalan, R. Belyansky, C. Wilson, and A. Lupascu, Ultrastrong coupling of a single artificial atom to an electromagnetic continuum in the nonperturbative regime, Nat. Phys. **13**, 39 (2017).
[38] J. Puertas Martínez, S. Léger, N. Gheeraert, R. Dassonneville, L. Planat, F. Foroughi, Y. Krupko, O. Buisson, C. Naud, W. Hasch-Guichard, S. Florens, I. Snyman, and N. Roch, A tunable Josephson platform to explore many-body quantum optics in circuit-QED, npj Quantum Inf. **5**, 19 (2019).
[39] S. Léger, J. Puertas-Martínez, K. Bharadwaj, R. Dassonneville, J. Delaforce, F. Foroughi, V. Milchakov, L. Planat, O. Buisson, C. Naud, W. Hasch-Guichard, S. Florens, I. Snyman, and N. Roch, Observation of quantum many-body effects due to zero point fluctuations in superconducting circuits, Nat. Commun. **10**, 5259 (2019).
[40] C. Ciuti, G. Bastard, and I. Carusotto, Quantum vacuum properties of the intersubband cavity polariton field, Phys. Rev. B **72**, 115303 (2005).
[41] R. Stassi, A. Ridolfo, O. Di Stefano, M. J. Hartmann, and S. Savasta, Spontaneous Conversion from Virtual to Real Photons in the Ultrastrong-Coupling Regime, Phys. Rev. Lett. **110**, 243601 (2013).
[42] Q.-K. He, Z. An, H.-J. Song, and D. L. Zhou, Generating photons from vacuum with counter rotating wave interaction, arXiv:1810.04523.
[43] N. Gheeraert, X. H. H. Zhang, T. Sépulcre, S. Bera, N. Roch, H. U. Baranger, and S. Florens, Particle production in ultrastrong-coupling waveguide QED, Phys. Rev. A **98**, 043816 (2018).
[44] E. Sánchez-Burillo, A. Cadarso, L. Martín-Moreno, J. J. García-Ripoll, and D. Zueco, Emergent causality and the *N*-photon scattering matrix in waveguide QED, New J. Phys. **20**, 013017 (2018).
[45] M. Cirio, K. Debnath, N. Lambert, and F. Nori, Amplified Optomechanical Transduction of Virtual Radiation Pressure, Phys. Rev. Lett. **119**, 053601 (2017).
[46] B. Peropadre, D. Zueco, D. Porras, and J. J. García-Ripoll, Nonequilibrium and Nonperturbative Dynamics of Ultrastrong Coupling in Open Lines, Phys. Rev. Lett. **111**, 243602 (2013).
[47] T. Shi, Y. Chang, and J. J. García-Ripoll, Ultrastrong Coupling Few-Photon Scattering Theory, Phys. Rev. Lett. **120**, 153602 (2018).
[48] E. Sanchez-Burillo, D. Zueco, J. J. Garcia-Ripoll, and L. Martin-Moreno, Scattering in the Ultrastrong Regime: Nonlinear Optics with One Photon, Phys. Rev. Lett. **113**, 263604 (2014).
[49] E. Sánchez-Burillo, J. García-Ripoll, L. Martín-Moreno, and D. Zueco, Nonlinear quantum optics in the (ultra)strong light-matter coupling, Faraday Discuss. **178**, 335 (2015).
[50] R. Stassi, V. Macrì, A. F. Kockum, O. Di Stefano, A. Miranowicz, S. Savasta, and F. Nori, Quantum nonlinear optics without photons, Phys. Rev. A **96**, 023818 (2017).
[51] A. F. Kockum, A. Miranowicz, V. Macrì, S. Savasta, and F. Nori, Deterministic quantum nonlinear optics with single atoms and virtual photons, Phys. Rev. A **95**, 063849 (2017).
[52] Z. Chen, Y. Wang, T. Li, L. Tian, Y. Qiu, K. Inomata, F. Yoshihara, S. Han, F. Nori, J. S. Tsai, and J. Q. You, Single-photon-driven high-order sideband transitions in an ultrastrongly coupled circuit-quantum-electrodynamics system, Phys. Rev. A **96**, 012325 (2017).
[53] A. F. Kockum, V. Macrì, L. Garziano, S. Savasta, and F. Nori, Frequency conversion in ultrastrong cavity QED, Sci. Rep. **7**, 5313 (2017).
[54] A. Frisk Kockum, A. Miranowicz, S. De Liberato, S. Savasta, and F. Nori, Ultrastrong coupling between light and matter, Nat. Rev. Phys. **1**, 19 (2019).
[55] P. Forn-Díaz, L. Lamata, E. Rico, J. Kono, and E. Solano, Ultrastrong coupling regimes of light-matter interaction, Rev. Mod. Phys. **91**, 025005 (2019).
[56] W. Ulrich, *Quantum Dissipative Systems*, 2nd ed., Series in Modern Condensed Matter Physics Vol. 10 (World Scientific, Singapore, 1999).
[57] J. Prior, A. W. Chin, S. F. Huelga, and M. B. Plenio, Efficient Simulation of Strong System-Environment Interactions, Phys. Rev. Lett. **105**, 050404 (2010).
[58] N. Lambert, S. Ahmed, M. Cirio, and F. Nori, Modelling the ultra-strongly coupled spin-boson model with unphysical modes, Nat. Commun. **10**, 3721 (2019).

[59] M. Grifoni and P. Hänggi, Driven quantum tunneling, Phys. Rep. **304**, 229 (1998).

[60] K. Le Hur, *Understanding Quantum Phase Transitions* (CRC, Boca Raton, 2010), pp. 245–268.

[61] T. Yokota, K. Masuki, and Y. Ashida, Functional renormalization group approach to circuit quantum electrodynamics, arXiv:2208.14107.

[62] E. Sánchez-Burillo, L. Martín-Moreno, J. J. García-Ripoll, and D. Zueco, Single Photons by Quenching the Vacuum, Phys. Rev. Lett. **123**, 013601 (2019).

[63] R. Silbey and R. A. Harris, Variational calculation of the dynamics of a two level system interacting with a bath, J. Chem. Phys. **80**, 2615 (1984).

[64] S. Bera, A. Nazir, A. W. Chin, H. U. Baranger, and S. Florens, Generalized multipolaron expansion for the spin-boson model: Environmental entanglement and the biased two-state system, Phys. Rev. B **90**, 075110 (2014).

[65] G. Díaz-Camacho, A. Bermudez, and J. J. García-Ripoll, Dynamical polaron *Ansatz*: A theoretical tool for the ultrastrong-coupling regime of circuit QED, Phys. Rev. A **93**, 043843 (2016).

[66] D. Zueco and J. García-Ripoll, Ultrastrongly dissipative quantum Rabi model, Phys. Rev. A **99**, 013807 (2019).

[67] Y. Ashida, T. Yokota, A. İmamoğlu, and E. Demler, Nonperturbative waveguide quantum electrodynamics, Phys. Rev. Res. **4**, 023194 (2022).

[68] T. Shi, E. Demler, and J. I. Cirac, Variational study of fermionic and bosonic systems with non-Gaussian states: Theory and applications, Ann. Phys. (NY) **390**, 245 (2018).

[69] D. D. Noachtar, J. Knörzer, and R. H. Jonsson, Nonperturbative treatment of giant atoms using chain transformations, Phys. Rev. A **106**, 013702 (2022).

[70] M. H. Devoret, in *Quantum Fluctuations*, edited by S. Reynaud, E. Giacobino, and J. Zinn-Justin, *Proceedings of the Les Houches Summer School of Theoretical Physics*, LXIII, 1995 (Elsevier, Amsterdam, 1997), pp. 351–386.

[71] A. J. Leggett, S. Chakravarty, A. T. Dorsey, M. P. A. Fisher, A. Garg, and W. Zwerger, Dynamics of the dissipative two-state system, Rev. Mod. Phys. **59**, 1 (1987).

[72] U. Weiss, *Quantum Dissipative Systems* (World Scientific, Singapore, 2012).

[73] J. Román-Roche, E. Sánchez-Burillo, and D. Zueco, Bound states in ultrastrong waveguide QED, Phys. Rev. A **102**, 023702 (2020).

[74] G. Díaz-Camacho, D. Porras, and J. J. García-Ripoll, Photon-mediated qubit interactions in one-dimensional discrete and continuous models, Phys. Rev. A **91**, 063828 (2015).

[75] H. Spohn and R. Dümcke, Quantum tunneling with dissipation and the Ising model over $\mathbb{R}$, J. Stat. Phys. **41**, 389 (1985).

[76] D. P. S. McCutcheon, A. Nazir, S. Bose, and A. J. Fisher, Separation-dependent localization in a two-impurity spin-boson model, Phys. Rev. B **81**, 235321 (2010).

[77] F. Guinea, E. Bascones, and M. J. Calderon, in *Lectures on the Physics of Highly Correlated Electron Systems and High-T_c Superconductors*, edited by F. Mancini, AIP Conf. Proc. No. 438 (AIP, Melville, 1998), p. 1.

[78] J. J. García Ripoll, *Quantum Information and Quantum Optics with Superconducting Circuits* (Cambridge University Press, Cambridge, 2022).